

CHEMISTRY

AN ASIAN JOURNAL

www.chemasianj.org

Accepted Article

Title: Electronic Structure of a Semi-conducting Imine-Covalent Organic Framework

Authors: Vipin Mishra, Vivek K. Yadav, Jayant K Singh, and Thiruvancheril Gopalakrishnan Gopakumar

This manuscript has been accepted after peer review and appears as an Accepted Article online prior to editing, proofing, and formal publication of the final Version of Record (VoR). This work is currently citable by using the Digital Object Identifier (DOI) given below. The VoR will be published online in Early View as soon as possible and may be different to this Accepted Article as a result of editing. Readers should obtain the VoR from the journal website shown below when it is published to ensure accuracy of information. The authors are responsible for the content of this Accepted Article.

To be cited as: *Chem. Asian J.* 10.1002/asia.201900586

Link to VoR: <http://dx.doi.org/10.1002/asia.201900586>

A Journal of



A sister journal of *Angewandte Chemie*
and *Chemistry* – A European Journal

WILEY-VCH

FULL PAPER

Electronic Structure of a Semi-conducting Imine-Covalent Organic Framework

Vipin Mishra,^[a] Vivek K. Yadav,^[b] Jayant K. Singh,^[b] and Thiruvancheril G. Gopakumar*^[a]

Abstract: Imine COF (covalent organic framework) based on Schiff base reaction between p-Phenylenediamine (PDA) and Benzene-1,3,5-tricarboxaldehyde (TCA) is prepared on the HOPG-air (air = humid N₂) interface and characterized using different probe microscopes. Role of the molar ratio of TCA and PDA has been explored, and smooth domains up to a few μm are formed for high TCA ratio (> 2) compared to PDA. It is also observed that the microscopic roughness of imine COF is strongly influenced by the presence of water (in the reaction chamber) during the Schiff base reaction. The electronic property of imine COF obtained by tunneling spectroscopy and dispersion corrected Density Functional Theory (DFT) calculation are comparable and show semiconducting nature with a band gap of ~ 1.8 eV. Further, we show that the frontier orbitals are delocalized entirely over the framework of imine COF. The calculated cohesive energy shows that the stability of imine COF is comparable to that of graphene.

Introduction

The magnificent upsurge in the area of 2D (two dimensional) materials comes with the emergence of graphene.[1] This aspired scientific community to look for novel 2D materials beyond graphene, like graphyne,[2] germanene,[3] MoS₂,[4] Boron Nitride (BN),[5] etc. Application based on these 2D materials[6] may play a pivotal role in the development of advanced thin and flexible electronics. To increase the applicability, it is vital to modify the electronic properties of these materials. Several methods have been proposed for graphene, which includes substrate[7], adsorption of atoms[8], doping of heteroatoms within the sheet[9, 6a] and so on. En-route to the development of 2D materials a new class has emerged where organic molecular building blocks are used to form covalently linked molecular 2D materials on surfaces. These 2D materials are generally referred to as covalent organic framework (COF).[10] Paramount advantage is the

potential for tailoring the electronic properties of 2D COF based on the selection of building blocks. One may choose building blocks predisposed with heteroatoms, which allows symmetric incorporation of them in the 2D COF. The vast variety of building blocks available in the molecular library is an added advantage. COF has been explored towards applications and properties like luminescence,[11] switching,[11a] electrical conductivity/charge carrier mobility,[12] thermal stability,[12] defect induced mobility[13], mechanical stability,[13] and oxidation induced conductivity[14,15] have been intensively studied. Electronically conjugated (sp² hybridization) COFs which are semiconducting in nature has been also demonstrated.[12,15]

Typically 2D COF is formed via chemical reactions like Ullmann coupling,[16] Schiff base reaction[17], triazine coupling[18] and ester linkage[19] on surfaces. 2D COFs have also been addressed using density functional theory (DFT) with van der Waals correction.[20] The effects of strain[21] and variation in the length of building blocks[22] on the nature of the band gap of COFs have been explored theoretically. It was also observed that the presence of graphene or inert substrate does not alter the electronic properties of COFs, which is the same as observed for gas phase calculations.[23]

While Schiff base coupling (imine linkage) reaction occurs at mild conditions, Ullmann's reaction occurs on catalytic surfaces (metal surfaces) and triazine coupling is possible at high temperature. Ease of equilibrating the reaction with water for self-repair of COF during its formation is an added advantage of Schiff's base reaction over the other methods. Though imine COF has been used for diverse applications like catalysis,[17f,18] sensing[24], the major challenge in the formation of COF using the above methods is its limited domain size. It is desirable to increase the size of 2D sheets for practical applications based on these materials.

In this article, we show that the domain size and microscopic quality of an imine COF[17b, 17c, 25] can be optimized by the ratio of building blocks. The building blocks of imine COF are p-Phenylenediamine (PDA) and Benzene-1,3,5-tricarboxaldehyde (TCA). Surprisingly, a higher ratio of aldehyde (> 2) favors the formation of uniform smooth domains of imine COF up to a few μm . A combination of Scanning Tunneling Microscope (STM), Atomic Force Microscope (AFM) and photoelectron spectroscopy (XPS) has been employed to prove the formation of imine COF unanimously. The electronic structure of the imine COF determined using tunneling spectroscopy and density functional theory (DFT) suggests that the imine COF is semiconducting in nature with a band gap of ~ 1.8 eV.

[a] Mr. Vipin Mishra and Dr. Thiruvancheril G. Gopakumar*
Department of chemistry
Indian Institute of Technology Kanpur,
Kanpur, UP – 208016, India
E-mail: gopan@iitk.ac.in

[b] Dr. Vivek K. Yadav and Prof. Jayant K. Singh
Department of chemical engineering
Indian Institute of Technology Kanpur,
Kanpur, UP – 208016, India
Email: jayantks@iitk.ac.in

Supporting information for this article is given via a link at the end of the document.

FULL PAPER

Results and Discussion

Figure 1(a) shows the formation of imine COF from TCA and PDA building blocks on the HOPG surface in the presence of water at ~ 230 °C. Figure 1(b-d) show typical constant force AFM topographs of imine COF formed at different ratios of TCA and PDA. Bright blue regions in all the images (Figure 1(b-d)) are the imine COF on HOPG (appears dark blue). White dashed lines depict a few terrace edges. Three different ratios of TCA and PDA have been used to form imine COF. Figure 1(b) shows COF formed by mixing TCA and PDA in the ratio of 1:3. Figure 1(c and d) show imine COF formed from 1:1 and 2:1 ratio of TCA and PDA. The imine COF formed from 1:3 ratio of TCA and PDA is rough as evident from the small and large fractures (indicated using green dotted lines). These fractures are distributed uniformly over the entire imine COF. Strikingly the imine COF appears more uniform as the TCA ratio increases. Uniform smooth regions of imine COF are indicated using the red dotted line in Figure 1(c,d). Particularly for the 2:1 ratio, the area of the smooth region of imine COF increases by many folds. We attribute these smooth uniform regions to be well-ordered domains of imine COF. The regions in between the uniform domains are attributed to defective imine COF or pristine graphite (green dotted lines). This indicates that increasing the proportion of TCA in the mixture of building blocks has a positive effect in the formation of large uniform domains of imine COF of the order of a few μm . S3 in the SI illustrates additional AFM images of imine COFs prepared at different mixing ratios and S4 in the SI shows large uniform domains of imine COF of the order of a few μm .

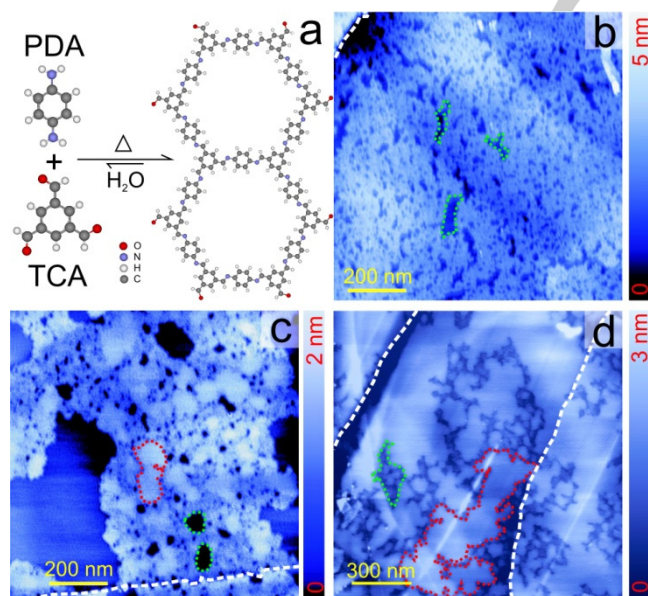


Figure 1. (a) Schematic of the preparation of imine COF from TCA and PDA in the presence of water. Constant force AFM Topography of imine COF formed from TCA and PDA at different molar mixing ratios, 1:3 (b), 1:1 (c) and 2:1 (d). The concentration of TCA and PDA was kept at $\sim 10^{-4}$ M, and the reaction was carried out at ~ 230 °C. Red dotted regions show uniform imine COF and green dotted regions show a few defects formed on HOPG. White dashed line represents a few graphite terrace edges.

Figure 2(a,b) show constant current STM topographs of imine COF formed from TCA and PDA (ratio 2:1) on HOPG-air interface at ambient conditions. The bright regions correspond to imine COF, and the dark blue regions are pristine graphite. White dashed line in figure 2(a) shows a graphite terrace edge. Figure 2(b) shows a moderately resolved topograph and the corresponding fast Fourier transform (2D-FFT) is included in the inset. The FFT shows clear, bright spots, which corresponds to a hexagonal pattern. The sharp spots indicate that the imine COF is uniform and have low defects. Figure S4 in the SI shows additional STM topograph with a large area (~ 1 μm) along with a moderately resolved part of the large domain. Figure 2(c) shows a mesh averaged image of COF obtained from a high-resolution topograph. Since imaging is performed at the solid-air interface,[17c] and therefore we use the mesh average image. The quality of the images are not as good as the reported solid-liquid interface,[17c] and therefore we use the mesh average image. $\vec{A} = \vec{B} = 2.35 \pm 0.17$ nm and $\alpha = 59 \pm 3^\circ$ represent the unit cell vectors and the angle between them, respectively. The unit cell vectors correspond to the expected COF unit cell. A theoretically calculated imine COF is overlaid on the mesh averaged image (Figure 2(c)), which matches very well with the experimental unit cell.

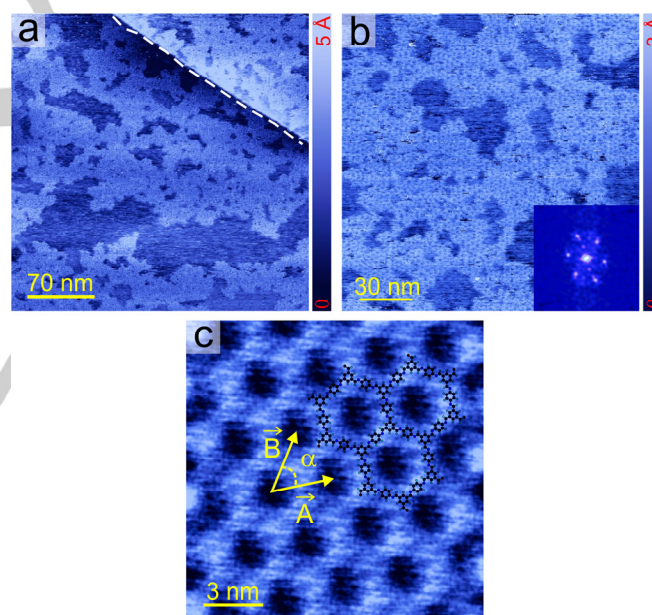


Figure 2. Constant current STM topographs (0.74 V, 40.0 pA) of imine COF obtained from 2:1 ratio of TCA and PDA. The concentration of TCA and PDA was kept at $\sim 10^{-4}$ M and the reaction was carried out at ~ 230 °C. (b) Further high resolution with the corresponding FFT of imine COF. (c) Mesh averaged STM image of a selected region of imine COF with overlaid theoretically optimized model. \vec{A} , \vec{B} and α are the lattice parameters of imine COF.

To ensure that the observed domains in both STM and AFM are not the assembly of unreacted molecules, we have carried out STM experiments of the mixture of TCA and PDA (for 1:1 molar ratio) on the surface without annealing. The topographs of the mixture reveal close-packed assembly of molecules (STM image is shown in SI S5). After annealing, we have not observed

For internal use, please do not delete. Submitted_Manuscript

FULL PAPER

domains with close-packed molecules (XPS also supports the above results, which will be discussed later) and the majority of the surface is covered by honeycomb pattern corresponding to COF.

To confirm the formation of imine COF we have performed XPS. Figure 3 shows the N1s XPS spectrum of imine COF (ratio 2:1) on HOPG. We have used C1s (sp^2) resonance from HOPG as a reference according to literature (~ 284.4 eV). The C1s spectrum is provided in S6 of SI. The spectrum is fitted with two Gaussian peaks with peak maxima at 399.07 eV and 400.68 eV. These resonances correspond to imine bond ($-N=C-$) and amine ($-NH_2$), respectively. The major resonance from imine indicates the formation of imine COF and the weak amine indicates unreacted precursor molecules. Near the C1s edge, we observe a shoulder corresponding to $-C=N-$ (285.2 eV, see S6 in the SI), which further confirms the formation of imine and therefore the imine COF. The XPS result is in agreement with previous reports.[17b, 17c, 34] The XPS spectra from 1:3 (TCA:PDA) ratio is included in S7 of the SI. N1s resonance in the XPS spectrum for 1:3 show indication of excess amine together with imine, which might be leading to the rougher surface and incomplete formation of imine COF.

We show using AFM, STM, and XPS that imine COF can be prepared on the HOPG-air interface. We show using AFM and XPS that the formation of imine COF is dependent on the ratio of the precursors. As we increase the ratio of TCA, smooth large domain of imine COF is forming up to a few μm . However, for high amine ratio (1:3) the domains of COF appears rather defective with uniformly distributed fractures. We also observed defect free domains of COF upto a few μm for a very high ratio of TCA (4:1) (corresponding AFM images in S3 of the SI). However, the overall percentage of the COF on the HOPG surface for this ratio decreases compared to that of 2:1 and 1:1 ratio. The dependence of the ratio of TCA and PDA in the formation of imine COF is striking. In general, one would expect the imine COF formation from 2:3 ratio of TCA and PDA according to the stoichiometric ratio of the reaction (cf. Figure 1(a)). Previous report also shows formation of imine COF at 2:3 ratio of TCA and PDA.[17g, 17h, 17i] High crystallinity is also observed for 1:1 molar ratio of the building blocks in Schiff base reaction.[11b] Our observation is, however, opposite to what is previously reported. We argue that possible desorption of TCA during the preparation (heating) leads to lowering of the actual amount of TCA on surface. Thus to maintain the stoichiometric ratio of the reaction higher ratio of TCA is required on the hot surface with respect to PDA. The defective imine COF obtained for higher amine ratio (expected stoichiometric ratio) may be justified due to excess of amine present on the surface (also observed in XPS, see S7 in the SI). We also note that the optimum temperature for the formation of imine COF in our case is higher than that of reported (~ 150 °C).[17b] This is possibly due to the different type of experimental set-up employed in our case compared to literature.

We also studied the effect of concentration of TCA and PDA in the working solutions. It is observed that imine COF prepared from higher concentration ($\sim 10^{-3}$ M) also produces smooth and defect free domains for high TCA ratio (4:1) compared to that

formed from the equimolar ratio (1:1). The COF formed at equimolar ratio of TCA and PDA shows rough morphology for the film with an average roughness of ~ 1.5 nm. This indicates possible multilayer formation. The XPS data corresponding to these films shows resonances related to $-C=N-$ linkages on the surface. The roughness together with $-C=N-$ linkages suggest that at high concentration of precursors, cross-linked multi-layer COF is formed. Corresponding AFM images with cross sectional line profile and XPS results are shown in SI S8.

We also note that increasing the temperature during the preparation of imine COF above optimum temperature produce rather rough and defective domains. AFM images of 4:1 imine COF prepared at ~ 300 °C is provided in S9 of the SI. This indicates that there exists a critical temperature for the imine COF formation on HOPG. For metallic surfaces, lower COF formation temperature has been reported,[16b,16c] where the catalytic effect of metal plays a role. To confirm the effect of water, we have prepared imine COF (2:1 ratio) without water and has yielded defective COF (AFM images are provided in S10 of the SI). The quality of the imine COF formed in the presence of water is in accordance with the equilibration of water in the chemical reaction and its role in correcting the defects formed during the reaction. Water vapour has been used previously for 2D COF preparation, to self-repair possible defects formed within the imine COF.[17c, 19g]

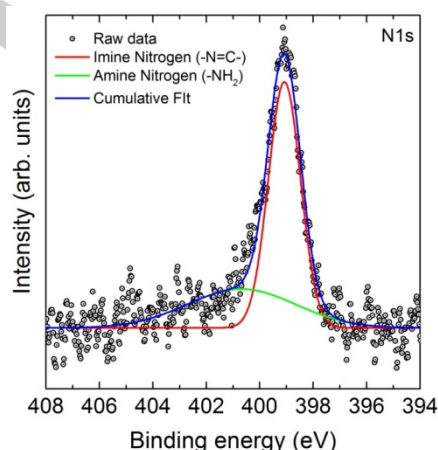


Figure 3. N1s resonances from XPS of imine COF obtained from 2:1 ratio of TCA and PDA on HOPG. The concentration of TCA and PDA was kept at $\sim 10^{-4}$ M and the reaction was carried out at ~ 230 °C. Independent Gaussian peaks correspond to imine ($-N=C-$) and amine ($-NH_2$) nitrogen.

Figure 4 shows a normalized differential conductivity (dI/dV) obtained from imine COF on HOPG using Scanning Tunneling Spectroscopy (STS). Three independent dI/dV spectra (each spectra is an average of ~ 30 measurements) are included. The normalization procedure is as follows. Simultaneously recorded dI/dV spectra on bare graphite is subtracted (using a factor) from dI/dV spectra obtained on imine COF. This procedure is implemented to reduce the influence of graphite density of states (DOS) (see details and raw dI/dV obtained on imine COF in S1 in

For internal use, please do not delete. Submitted_Manuscript

FULL PAPER

the SI). The raw dI/dV spectra obtained from imine COF on HOPG has zero band gap and is due to the influence of the DOS of graphite. The dI/dV spectra typically represent local DOS of a sample near the Fermi energy. We observe a clear band gap (a region with no DOS) near the Fermi energy in the dI/dV spectra measured on imine COF after normalization. The band gap is ~ 1.8 eV; the onsets of valance and conduction band edges are indicated with red dashed lines. The bandgap is asymmetric around the Fermi energy. Semiconducting COF has been reported previously using different molecular precursors.[20]

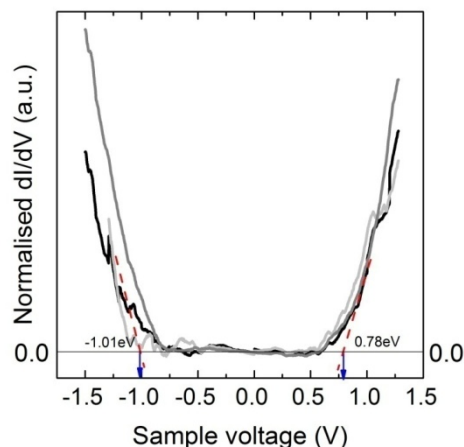


Figure 4. Differential conductivity (dI/dV) recorded on imine COF on HOPG surface (same as in Figure 2). Three dI/dV spectra (black, dark grey and light grey) represent three averaged independent measurements on imine COF.

To understand the stability and the electronic structure of imine COF on graphite, we employed the first principle density functional theory (DFT) approach. The structure of imine COF after relaxation/optimization on bilayer graphite shows that both imine COF layer and graphite retain their planarity (see S11 in the SI). Top view of the imine COF extracted from the calculation is overlaid in Figure 2(c), which shows an excellent agreement with experimentally obtained lattice parameters. S11 in the SI provide side view, lattice parameters, and unit cell of the imine COF. The presence of graphite ensures the COF retains its planar geometry without any rippling. This is evident from the computed C-C and C-N bond lengths for the bare COF and the COF on graphite, which shows only slight variations in the bond lengths (less than 0.01, see details in Table-S1 in the SI). The average distance between the COF and the top layer of graphite is 3.40 Å, whereas the graphite inter-layer distance is found to be 3.31 Å. The computed distances fall in the range of van der Waals interaction. We further calculated the binding energy E_b of COF on graphite using the following equation.

$$E_b = E_{(\text{COF}+\text{Graphite})} - (E_{\text{COF}} + E_{\text{Graphite}})$$

where $E_{(\text{COF}+\text{Graphite})}$ represents the total energy of the system, E_{Graphite} is the total energy of the graphite sheet and E_{COF} denotes

the energy of COF in the gas phase. The calculated binding energy (E_b) for imine COF on graphite is -2.14 eV and -2.06 eV per unit cell for PBE and BLYP, respectively. The structural and thermodynamic stability of imine COF is analyzed by calculating their cohesive energy. The cohesive energy (6.84 eV (PBE) and 6.25 eV (BLYP)) shows that the imine COF is forming a stable structure in comparison to graphene (~ 7.8 eV).[35]

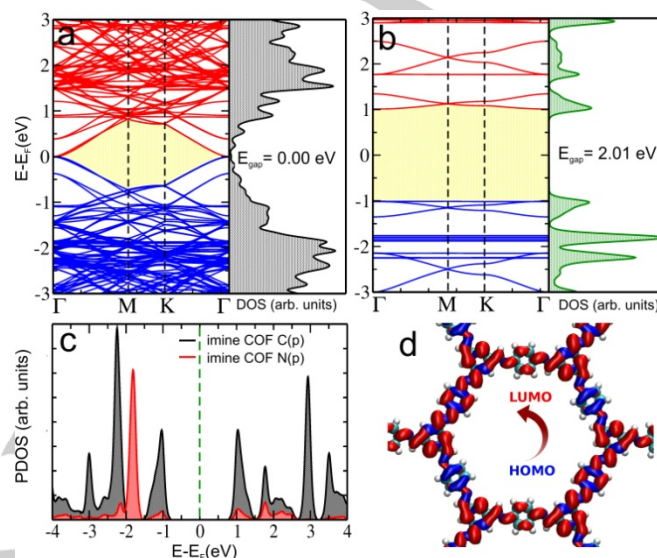


Figure 5: Band structure and total density of states (DOS) of imine COF with graphite (a) and that of imine COF (b). (c) Partial density of states (PDOS) for imine COF; p-orbital contribution from C and N are shown. The Fermi level is set at 0 eV. (d) Charge density isosurface of the HOMO (blue) and LUMO (red) of the imine COF. The isosurface value is set to $0.001 \text{ e} \text{ \AA}^{-1}$

Next, we investigate the electronic structure of imine COF. The band structure and the density of states (DOS) of the imine COF on graphite and imine COF alone are presented in Figure 5 a and b, respectively. The band structure and total density of state of the graphite, imine COF and imine COF with graphite is shown in S12 in the SI for comparison. The k-path selection produces similar band structure (with gamma point as a minimum) as shown in the previous report[25] and the corresponding reciprocal lattice is included in S11 in the SI. The imine COF with graphite shows a dispersive band gap (i.e., zero band gap), whereas imine COF alone shows flat band-gap near the Fermi energy. The DOS for imine COF on graphite is dominated by graphene-like behaviour near the Fermi level with a band gap of ~ 0.00 eV. The DOS of imine COF alone shows a striking difference and has a band gap (HOMO-LUMO) of 2.01 (1.95) eV for PBE (BLYP) functionals. This band gap is in good agreement with the experimentally obtained band gap using tunneling spectroscopy (cf. figure 4). In addition, the band gap is also asymmetric around the Fermi energy as see in the experiments. In Figure 5c, we have plotted the partial density of state (PDOS) for the imine COF. PDOS exhibits that the HOMO and LUMO of imine COF are dominated by the p-orbitals of the carbon atoms. For imine COF, the charge density isosurface of the HOMO and LUMO are displayed in

For internal use, please do not delete. Submitted_Manuscript

FULL PAPER

Figure 5d. The charge density isosurface of the HOMO and LUMO are separately shown in S13 of the SI. It is clear from Figure 5(d) that the electron density is delocalized over the entire imine COF. We also notice that frontier bands of imine COF are decoupled from the graphite band. However, there is a signature of significant mixing of valance and conduction bands (below valance-2 and above conduction+2 bands) of imine COF with graphite bands. Decoupling of electronic states at COF-graphene-inert surfaces has been shown previously.[23] Thus, we conclude that imine COF displays semiconducting behavior.

Conclusions

We have prepared imine linked COF from p-phenylenediamine (PDA) and benzene-1,3,5-tricarboxaldehyde (TCA) on HOPG. Microscopic structural and electronic characterization has been performed using AFM and STM, and the results are compared to that of first principle DFT calculations. The domain size of imine COF is controlled using the molar ratio and concentration of building blocks. The high molar ratio of TCA (> 2) promotes smooth growth of imine COF up to a few μm large domains. Additionally, we observe that there is a critical temperature ($> 230\text{ }^\circ\text{C}$) for the formation of smooth defect-free domains of imine COF. Presence of water during the reaction also favours the formation of smooth imine COF, which regulates a backward reaction and repairs the defects. XPS further supports the formation of imine COF. The electronic properties obtained by DFT calculations show good agreement with the experiments. It is observed that the imine COF is semiconducting in nature with a band gap of $\sim 1.8\text{ eV}$. The calculation also shows that the frontier orbitals of imine COF are delocalized on the network, which suggests that it may be used in optoelectronic applications. The calculated cohesive energy indicates high stability of imine COF, which is comparable to that of graphene.

Experimental Section

Thin Film Preparation and experimental characterization: TCA (purity $\geq 99\%$) and PDA (purity $\geq 99\%$) purchased from Sigma Aldrich are used for the experiments with no further purification. The solutions are prepared using methanol (HPLC grade, $\geq 99.9\%$) obtained from Merck. TCA and PDA molecules are dissolved in methanol (concentration $\sim 10^{-4}\text{ M}$) and sonicated for 10 minutes to ensure homogeneous solvation. An equimolar concentration of TCA and PDA are mixed in the ratio 1:3 to 4:1 (TCA:PDA) and drop-casted ($\sim 2\ \mu\text{l}$) on freshly cleaved HOPG surface. The drop-casted HOPG is transferred to a reaction chamber (round bottom flask made up of Borosil glass with rubber stopper), which has a continuous supply of N_2 gas moistened with water (HPLC grade). The reaction chamber is heated (on hot plate) to a temperature of $\sim 230\text{ }^\circ\text{C}$ for 5 hours. This sample is used for the STM, AFM and XPS measurements at ambient condition. RHK STM and Agilent-5500 AFM are used for samples analysis. Mechanically cut Pt/Ir wire is used as STM tips. We have used intermittent contact mode AFM (also referred to as AC Mode due to alternating contact of the tip to the surface). AFM images are obtained using PPP-NCH silicon cantilevers purchased from Nanosensors ($\sim 310\text{ kHz}$, $\sim 35\text{ N/m}$), which are designed for intermittent contact mode of operation. A feedback system is employed to maintain the oscillation amplitude at a set point

value. The difference between the amplitude and set-point called the "error signal" is used as the input of the feedback system. The average force is maintained constant during the measurement. All the AFM and STM images are post-processed and analyzed using WSxM [26] software. XPS experiments are performed in UHV PHI 5000 Versa Prob II. The binding energy scale calibration was verified using the substrate C1s (284.4 eV) energy level. dI/dV spectra are measured using a lock in amplifier. Sin wave with average voltage of 100 mV (peak to peak) is used for modulation.

Computational Details: Theoretical calculations are performed using first-principles density functional theory (DFT) as implemented in the Quantum ESPRESSO code[27]. We used a generalized gradient approximation (GGA) with the Perdew-Burke-Ernzerhof (PBE) [28] parameterization of the exchange-correlation energy functional with ultrasoft pseudo potentials[29]. The Köhn-Sham wave-functions are expanded by plane wave basis set with a kinetic energy cut-off of 35 Ry. Brillouin zone (BZ) integration was done using a uniform Monkhorst-Pack[30] with a k-point grid of $5 \times 5 \times 1$ for geometry optimization and $10 \times 10 \times 1$ for electronic structure calculations. We have performed benchmark calculations in order to check the converged values for cut-off energy and K-points as shown in Figure S2 in the SI. The structures were relaxed until the magnitude of the Hellman-Feynman force on each ion became smaller than 0.03 eV/\AA . To nullify the interaction between periodic images, a large vacuum of 20 Å was employed in a direction perpendicular to the sheet (along the z-axis). The unit of the system for the calculation composed of COF (66 atoms) over bilayer graphite (324 atoms). For analysis, we ran two sets of simulation, one COF with graphite and another one with only COF, using PBE[28] and BLYP[16] functionals, respectively. A recent report shows that the implementation of vdW interaction is detrimental to adsorption energies.[25] Thus, we have used Grimme's dispersion correction to DFT calculations; DFT-D3[32] for PBE and DFT-D2 [33] for BLYP functional.

Acknowledgements

The authors would like to thank the Ministry of Electronics and Information Technology (MeitY) for providing the infrastructure grant through the Visvesvaraya Ph.D. Programme. V.M. would like to thank the Council of Scientific and Industrial Research (CSIR) for the research fellowship. This work is also supported by the department of science and technology, SERB (grant no: SB/S3/CE/079/2015). The calculations were partly done at the High-Performance Computing (HPC13) Facility at Computer Centre, IIT Kanpur.

Keywords: 2D covalent organic framework • Molecular materials • Scanning Probe Microscopy • Photoelectron spectroscopy • Electronic structure

References

- [1] A. K. Geim, K. S. Novoselov, The rise of graphene, *Nat. Mater.* **2007**, 6, 183.
- [2] J. Kang, Z. Wei, J. Li, *ACS Appl. Mater. Interfaces* **2019**, 11, 2692-2706.
- [3] M. E. Davila, L. Xian, S. Cahangirov, A. Rubio, G. L. Lay, *New Journal of Physics* **2014**, 16, 095002.
- [4] K. F. Mak, C. Lee, J. Hone, J. Shan, T. F. Heinz, *Phys. Rev. Lett.* **2010**, 105, 136805.
- [5] L. Ci, L. Song, C. Jin, D. Jariwala, D. Wu, Y. Li, A. Srivastava, Z. F. Wang, K. Storr, L. Balicas, F. Liu, P. M. Ajayan, *Nat. Mater.* **2010**, 9, 430.

For internal use, please do not delete. Submitted_Manuscript

FULL PAPER

- [6] a) S. Feng, M. C. dos Santos, B. R. Carvalho, R. Lv, Q. Li, K. Fujisawa, A. L. Elias, Y. Lei, N. Perea-López, M. Endo, M. Pan, M. A. Pimenta, M. Terrones, *Sci. Adv.* **2016**, *2*, 7; b) Z. Li, M. Smeu, A. Rives, V. Maraval, R. Chauvin, M. A. Ratner, E. Borguet, *Nat. Commun.* **2015**, *6*, 6321; c) C. Cui, F. Xue, W.-J. Hu, L.-J. Li, *NPJ 2D Mater. Appl.* **2018**, *2*, 18.
- [7] S. Y. Zhou, G. H. Gweon, A. V. Fedorov, P. N. First, W. A. de Heer, D.-H. Lee, F. Guinea, A. H. Castro Neto, A. Lanzara, *Nat. Mater.* **2007**, *6*, 770.
- [8] R. Balog, B. Jorgensen, L. Nilsson, M. Andersen, E. Rienks, M. Bianchi, M. Fanetti, E. Laegsgaard, A. Baraldi, S. Lizzit, Z. Slijvančanin, F. Besenbacher, B. Hammer, T. G. Pedersen, P. Hofmann, L. Hornekaer, *Nat. Mater.* **2010**, *9*, 315.
- [9] X. Wang, X. Li, L. Zhang, Y. Yoon, P. K. Weber, H. Wang, J. Guo, H. Dai, *Science* **2009**, *324*, 768–771.
- [10] a) M. Dogru, T. Bein, *Chem. Commun.* **2014**, *50*, 5531–5546; b) J. W. Colson, A. R. Woll, A. Mukherjee, M. P. Levendorf, E. L. Spittler, V. B. Shields, M. G. Spencer, J. Park, W. R. Dichtel, *Science* **2011**, *332*, 228–231; c) E. Jin, M. Asada, Q. Xu, S. Dalapati, M. A. Addicoat, M. A. Brady, H. Xu, T. Nakamura, T. Heine, Q. Chen, D. Jiang, *Science* **2017**, *357*, 673–676; d) R. P. Bisbey, W. R. Dichtel, *ACS Cent. Sci.* **2017**, *3*, 533–543; e) S. Chandra, D. Roy Chowdhury, M. Addicoat, T. Heine, A. Paul, R. Banerjee, *Chem. Mater.* **2017**, *29*, 2074–2080; f) X. Li, Q. Gao, J. Wang, Y. Chen, Z.-H. Chen, H.-S. Xu, W. Tang, K. Leng, G.-H. Ning, J. Wu, Q.-H. Xu, S. Y. Quek, Y. Lu, K. P. Loh, *Nat. Commun.* **2018**, *9*, 2335;
- [11] a) S. Wan, J. Guo, J. Kim, H. Ihee, D. Jiang, *Angew. Chem.* **2008**, *120*, 8958; b) D. D. Medina, T. Sick, T. Bein, *Adv. Energy Mater.* **2017**, *7*, 1700387.
- [12] S. Wan, F. Gándara, A. Asano, H. Furukawa, A. Saeki, S. K. Dey, L. Liao, M. W. Ambrogio, Y. Y. Botros, X. Duan, S. Seki, J. F. Stoddart, O. M. Yaghi, *Chem. Mater.* **2011**, *23*, 4094.
- [13] J. I. Feldblyum, C. H. McCreery, S. C. Andrews, T. Kurosawa, E. J. G. Santos, V. Duong, L. Fang, A. L. Ayznerb, Z. Bao, *Chem. Commun.* **2015**, *51*, 13894.
- [14] S. Jin, T. Sakurai, T. Kowalczyk, S. Dalapati, F. Xu, H. Wei, X. Chen, J. Gao, S. Seki, S. Irlé, D. Jiang, *Chem. Eur. J.* **2014**, *20*, 14608.
- [15] E. Jin, M. Asada, Q. Xu, S. Dalapati, M. A. Addicoat, M. A. Brady, H. Xu, T. Nakamura, T. Heine, Q. Chen, D. Jiang, *Science* **2017**, *357*, 673.
- [16] a) J. Eichhorn, D. Nieckarz, O. Ochs, D. Samanta, M. Schmittl, P. J. Szabalski, M. Lackinger, *ACS Nano* **2014**, *8*, 7880–7889; b) A. Rastgoo-Lahrood, J. Björk, W. M. Heckl, M. Lackinger, *Chem. Commun.* **2015**, *51*, 13301–13304; c) B. Dennis, G. Hong-Ying, H. P. Alexander, S. Armido, F. Harald, D. N. L., N. Johannes, *Chem. Eur. J.* **2017**, *23*, 6190–6197; d) R. C. Quardokus, V. K. Tewary, F. W. DelRio, *Nanotechnology* **2016**, *27*, 442501; e) P. T. Anh, S. Fei, N. Manh-Thuong, L. Zheshen, S. Florian, S. Meike, *Chem. Eur. J.* **2016**, *22*, 5937–5944; f) C. J. Judd, S. L. Haddow, N. R. Champness, A. Saywell, *Sci. Rep.* **2017**, *7*, 14541; g) M. Lischka, M. Fritton, J. Eichhorn, V. S. Vyas, T. Strunskus, B. V. Lotsch, J. Björk, W. M. Heckl, M. Lackinger, *J. Phys. Chem. C* **2018**, *122*, 5967–5977; h) M. Lackinger, *Chem. Commun.* **2017**, *53*, 7872–7885; i) A. Rastgoo-Lahrood, M. Lischka, J. Eichhorn, D. Samanta, M. Schmittl, W. M. Heckl, M. Lackinger, *Nanoscale* **2017**, *9*, 4995–5001.
- [17] a) S.-Y. Ding, J. Gao, Q. Wang, Y. Zhang, W.-G. Song, C.-Y. Su, W. Wang, *J. Am. Chem. Soc.* **2011**, *133*, 19816–19822; b) X.-H. Liu, C.-Z. Guan, S.-Y. Ding, W. Wang, H.-J. Yan, D. Wang, L.-J. Wan, *J. Am. Chem. Soc.* **2013**, *135*, 10470–10474; c) Y. Yu, J. Lin, Y. Wang, Q. Zeng, S. Lei, *Chem. Commun.* **2016**, *52*, 6609–6612; d) Y. Yu, L. Yang, C. Liu, W. Q. Tian, Y. Wang, S. Lei, *Chem. Commun.* **2016**, *52*, 8317–8320; e) Y. Yu, J. Sun, S. Lei, *J. Phys. Chem. C* **2015**, *119*, 16777–16784; f) J. M. C. Cifuentes, B. X. Ferreira, P. M. Esteves, C. D. Buarque, *Topics in Catalysis* **2018**, *61*, 689–698; g) L. Xu, X. Zhou, Y. Yu, W. Q. Tian, J. Ma, S. Le, *ACS Nano* **2013**, *7*, 8066–8073; h) J. L. Segura, M. J. Mancheño, F. Zamora, *Chem. Soc. Rev.* **2016**, *45*, 5635; i) H. Wang, B. He, F. Liu, C. Stevens, M. A. Brady, S. Cai, C. Wang, T. P. Russell, T.-W. Tan, Y. Liu, *J. Mater. Chem. C*, **2017**, *5*, 5090.
- [18] X. Jiang, P. Wang, J. Zhao, *J. Mater. Chem. A* **2015**, *3*, 7750–7758.
- [19] a) L. Chunhua, Y. Yanxia, Z. Wei, Z. Qingdao, L. Shengbin, *Chem. Eur. J.* **2016**, *22*, 18412–18418. b) L. Chunhua, Z. Wei, Z. Qingdao, L. Shengbin, *Chem. Eur. J.* **2016**, *22*, 6768–6773; c) D. Cui, J. M. MacLeod, M. Ebrahimi, D. F. Perepichka, F. Rosei, *Chem. Commun.* **2015**, *51*, 16510–16513; d) J. F. Dienstmaier, A. M. Gigler, A. J. Goetz, P. Knochel, T. Bein, A. Lyapin, S. Reichmaier, W. M. Heckl, M. Lackinger, *ACS Nano* **2011**, *5*, 9737–9745; e) J. F. Dienstmaier, D. D. Medina, M. Dogru, P. Knochel, T. Bein, W. M. Heckl, M. Lackinger, *ACS Nano* **2012**, *6*, 7234–7242; f) J. Plas, O. Ivashenko, N. Martsinovich, M. Lackinger, S. De Feyter, *Chem. Commun.* **2016**, *52*, 68–71; g) S. Spitzer, A. Rastgoo-Lahrood, K. Macknapp, V. Ritter, S. Sotier, W. M. Heckl, M. Lackinger, *Chem. Commun.* **2017**, *53*, 5147–5150.
- [20] P. Zhu, V. Meunier, *J. Chem. Phys.* **2012**, *137*, 244703.
- [21] a) S.-M. Choi, S.-H. Jhi, Y.-W. Son, *Phys. Rev. B* **2010**, *81*, 081407; b) P. Logan, X. Peng, *Phys. Rev. B* **2009**, *80*, 115322; c) H. Zhao, K. Min, N. R. Aluru, *Nano Lett.* **2009**, *9*, 3012–3015.
- [22] L.-M. Yang, E. Ganz, S. Wang, X.-J. Li, T. Frauenheim, *J. Mater. Chem. C* **2015**, *3*, 2244–2254.
- [23] a) O. J. Silveira, S. S. Alexandre, H. Chacham, *J. Phys. Chem. C* **2016**, *120*, 19796–19803; b) Y. Zhou, Z. Wang, P. Yang, X. Zu, F. Gao, *J. Mater. Chem.* **2012**, *22*, 16964–16970; c) C. Chen, T. Joshi, H. Li, A. D. Chavez, Z. Pedramrazi, P.-N. Liu, H. Li, W. R. Dichtel, J.-L. Bredas, M. F. Crommie, *ACS Nano* **2018**, *12*, 385–391.
- [24] Q. Gao, X. Li, G.-H. Ning, K. Leng, B. Tian, C. Liu, W. Tang, H.-S. Xu, K. P. Loh, *Chem. Commun.* **2018**, *54*, 2349–2352; b) J. L. Segura, M. J. Mancheno, F. Zamora, *Chem. Soc. Rev.* **2016**, *45*, 5635–5671; c) S.-Y. Ding, W. Wang, *Chem. Soc. Rev.* **2013**, *42*, 548–568.
- [25] X. Lirong, Z. Xin, T. W. Quan, G. Teng, Z. Y. Feng, L. Shengbin, L. Z. Fan, *Angew. Chem. Int. Ed.* **2014**, *53*, 9564–9568.
- [26] I. Horcas, R. Fernández, J. M. Gómez-Rodríguez, J. Colchero, J. Gómez-Herrero, A. M. Baro, *Rev. Sci. Instrum.* **2007**, *78*, 013705.
- [27] P. Giannozzi, S. Baroni, N. Bonini, M. Calandra, R. Car, C. Cavazzoni, D. Ceresoli, G. Chiarotti, M. Cococcioni, I. Dabo, A. Dal Corso, S. Fabris, G. Fratesi, S. de Gironcoli, R. Gebauer, U. Gerstmann, C. Gougousis, A. Kokalj, M. Lazzeri, L. Martin-Samos, M. Marzari, F. Mauri, R. Mazzarello, S. Paolini, A. Pasquarello, L. Paulatto, C. Sbraccia, S. Scandolo, G. Scialuzero, A. Seitsonen, A. Smogunov, P. Umari, R. Wentzcovitch, *J. Phys.: Condens. Matter* **2009**, *21*, 395502.
- [28] J. P. Perdew, K. Burke, M. Ernzerhof, *Phys. Rev. Lett.* **1997**, *78*, 1396–1396.
- [29] D. Vanderbilt, *Phys. Rev. B* **1990**, *41*, 7892–7895.
- [30] H. J. Monkhorst, J. D. Pack, *Phys. Rev. B* **1976**, *13*, 5188–5192.
- [31] a) A. D. Becke, *Phys. Rev. A* **1988**, *38*, 3098–3100; b) C. Lee, W. Yang, R. G. Parr, *Phys. Rev. B* **1988**, *37*, 785–789.
- [32] S. Grimme, J. Antony, S. Ehrlich, H. Krieg, *J. Chem. Phys.* **2010**, *132*, 154104.
- [33] G. Stefan, *J. Comput. Chem.* **2006**, *27*, 1787–1799; b) J. c. v. Klimeš, D. R. Bowler, A. Michaelides, *Phys. Rev. B* **2011**, *83*, 195131.
- [34] C. Maddi, F. Bourquard, V. Barnier, J. Avila, M.-C. Asensio, T. Tite, C. Donnet, F. Garrelie, *Sci. Rep.* **2018**, *8*, 3247.
- [35] H. Shin, S. Kang, J. Koo, H. Lee, J. Kim, Y. Kwon, *J. Chem. Phys.* **2014**, *140*, 114702.

For internal use, please do not delete. Submitted Manuscript

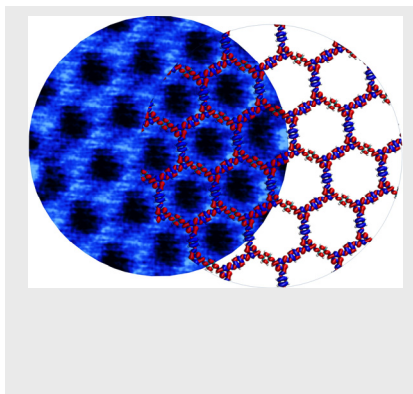
FULL PAPER

Entry for the Table of Contents (Please choose one layout)

Layout 1:

FULL PAPER

Semi-conducting 2D covalent organic framework



Vipin Mishra,^[a] Vivek K Yadav,^[b] Jayant K. Singh,^[b] and Thiruvancheril G. Gopakumar^{*[a]}

Page No. – Page No.

Title: Electronic Structure of a Semi-conducting Imine-Covalent Organic Framework